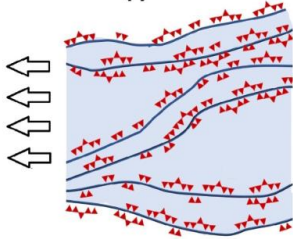
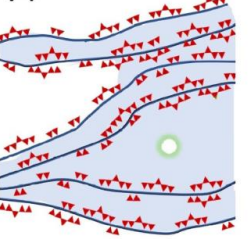
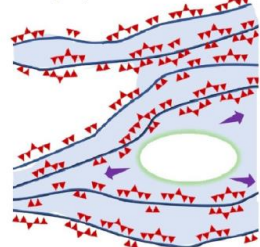
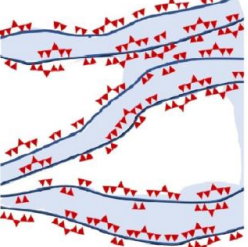
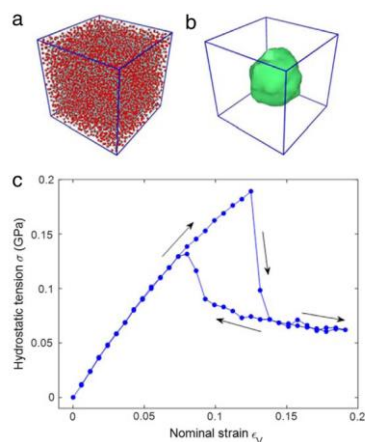


#	Short intro	Setup details	Outcomes	Related to us
<u>1</u>	<ul style="list-style-type: none">drying cementitious materials via classical nucleation theory using water desorption isothermshydrophobic ($\Theta > 120^\circ$)	Experimental	observed large moisture loss at $0.3\ p_v/p_{sat}$ can be explained by homogeneous cavitation	<div><div><div><div><div>(i)</div></div><div><div>(ii)</div></div></div><div><div><div>(iii)</div></div><div><div>(iv)</div></div></div></div><p>Proposed homogeneous cavitation event in C-S-H, black arrows represent the drying front, (i) saturated C-S-H(ii) drying occurs first in gel pores and in pores connected to the gel pores by receding meniscus (iii) Bubble expansion in the gel pore due to induced tensile pull when reaching $p_v/p_{sat} = 0.3$ (iv) drying by cavitation has occurred.</p></div>

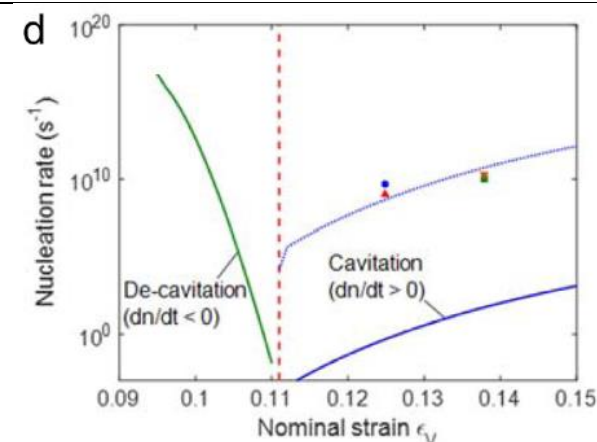
- molecular dynamics simulations to study cavitation of water under volume-controlled stretching
- proposed a modified nucleation theory



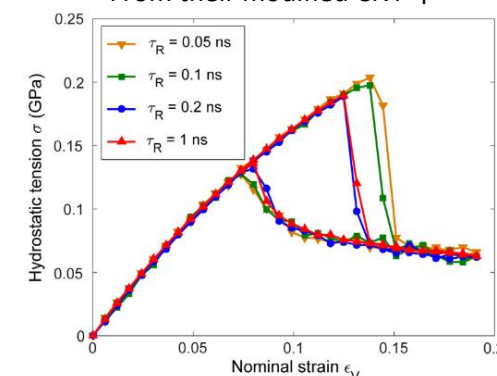
TIP4P/2005 model
Bulk: cubic box of water molecules with periodic boundary conditions
NPT, then NVT
Stretching: three dimensions simultaneously with $\Delta L = L_0 \Delta \epsilon$, where $\Delta \epsilon = 0.002$. (relax: 0.2ns)

- if decreasing the relaxation time to 0.1 and 0.05 ns, the onset of cavitation is slightly delayed till a higher strain and correspondingly a higher magnitude for the cavitation pressure (related to the nucleation rate)
- The average stress after cavitation depends on the initial volume

Related to us

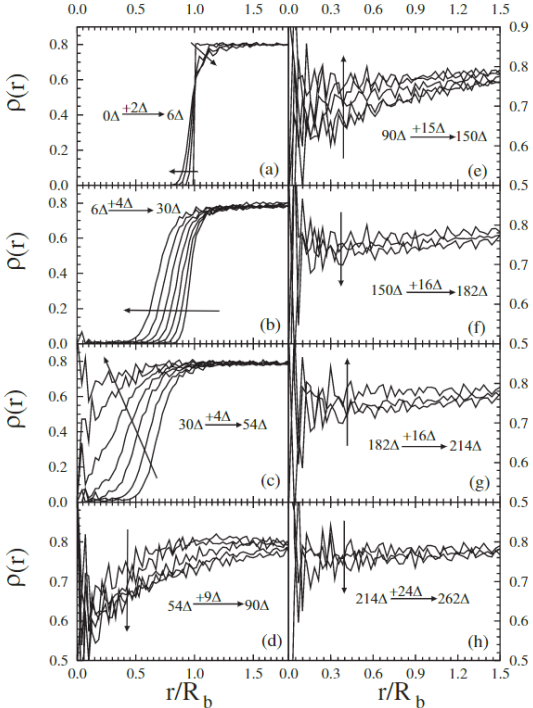
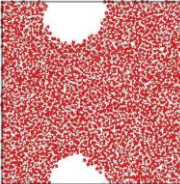


From their modified CNT ↑

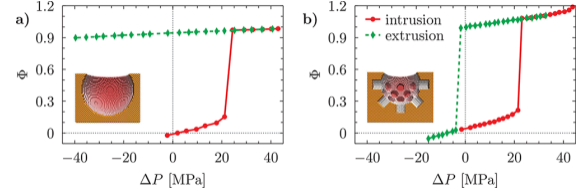
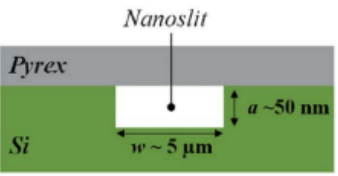
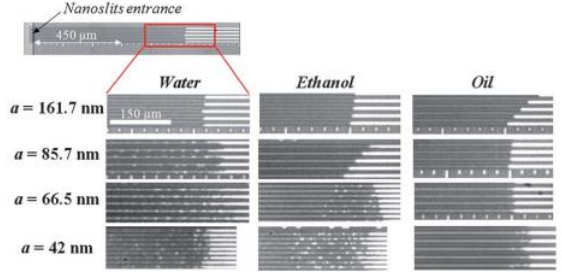


Effect of relaxation time ↑

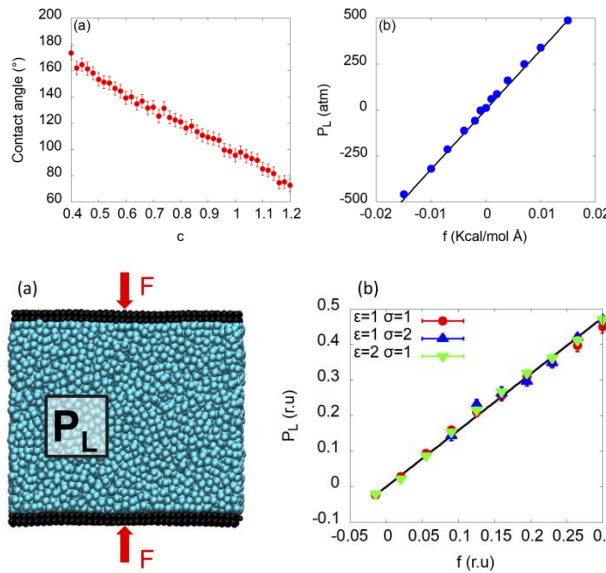
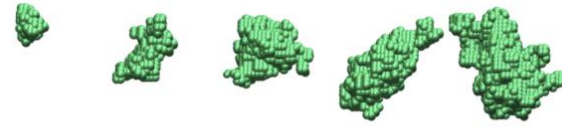
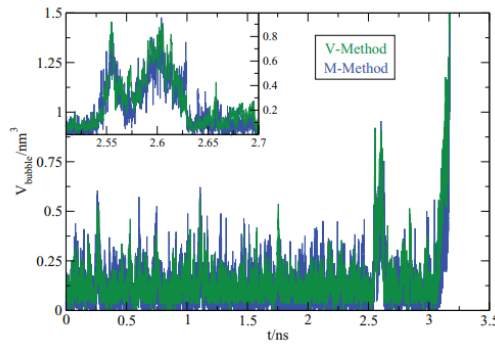
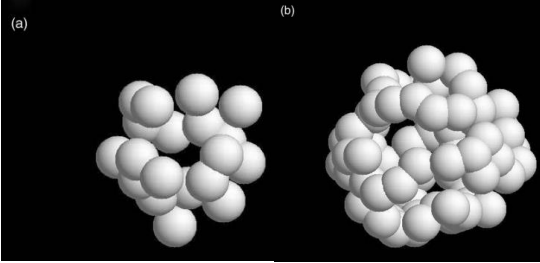
This document summarizes simulations/experimental setups in literature marking original targets and useful information.

#	Short intro	Setup details	Outcomes	Related to us
3	<ul style="list-style-type: none"> final stages of the collapse of an unstable cavity or bubble using the Molecular Dynamics 	<ul style="list-style-type: none"> spherical volume of molecules was removed from a bulk at the centre of the cubic simulation box 	<ul style="list-style-type: none"> temperature of individual molecules inside the cavity could reach at least an order of magnitude larger than that of the surrounding liquid, e.g., equivalent to 6,000 K for water. the bubble partially filled in, and then proceeded to partially empty again, and so on in an oscillatory manner 	 <p>$r=0$ is center of bubble. $\Delta=25\Delta t$, $\Delta t=0.125(\text{m}/\epsilon)^{0.5}$.</p> <ol style="list-style-type: none"> interface relaxes and becomes more spread out interface advances steadily towards centre of al-most empty cavity bubble fills up rapidly bubble emained about half-filled for a while and then started to empty again
4	<ul style="list-style-type: none"> volume-controlled stretching 	<ul style="list-style-type: none"> TIP4P/2005f box with 3D periodic boundary conditions NPT, then NVT (relax: 1ns) Stretching: initial density = 1.00035 g/cm³, then 0.898, 0.873, and 0.852 g/cm³ 	<ul style="list-style-type: none"> the breaking of hydrogen bonds promoted bubble generation and growth O-H bond could release energy to increase the amount of potential energy, so that cavitation was more likely to occur Once cavitation occurred, the O-H bond could absorb energy to reduce the amount of potential energy in the system, which will promote the 	 <ul style="list-style-type: none"> a rigid water model and do not take the effects of intermolecular vibrations

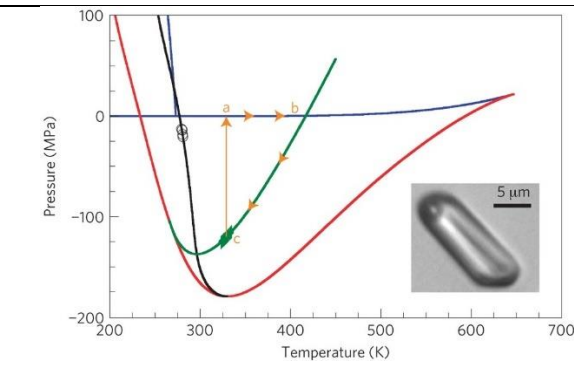
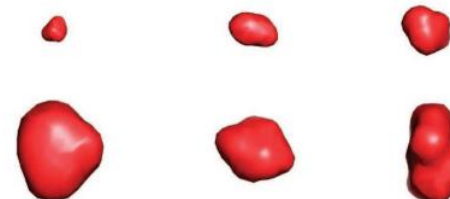
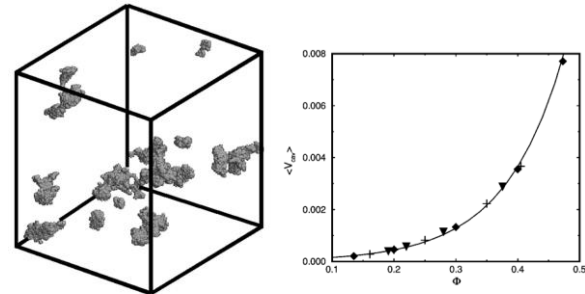
This document summarizes simulations/experimental setups in literature marking original targets and useful information.

#	Short intro	Setup details	Outcomes	Related to us
5	<ul style="list-style-type: none"> pore morphology on spontaneous extrusion of nonwetting liquids hydrophobic 	<ul style="list-style-type: none"> pore excavated from a LJ fcc crystal TIP4P-Ew water PNAS: $c=0.85$, $\Theta=115^\circ$ NPT, $p=\text{piston}$ – upper wall can move y in the wall-normal direction $A_p P_l = f N_p$, where A_p and N_p are the area and number of particles of the piston, respectively, and P_l is the water pressure 	<ul style="list-style-type: none"> the presence of small-scale roughness or pore interconnections this mechanism is generic and rooted in the pore topology 	 <ul style="list-style-type: none"> $\Delta P \approx P_l$
6	<ul style="list-style-type: none"> the role of gas on the capillary filling kinetics slowdown in nanoslits (depth going from 20 nm to 400 nm) trapped bubbles during a nanoslits capillary filling with water, ethanol, and silicone oil in silicon glass nanochannels glassy silica is typically hydrophilic under ambient conditions Stagnant trapped bubbles lifetime is investigated 		<ul style="list-style-type: none"> Bubbles are trapped only when slit depth is below a liquid-dependent threshold trapping of bubbles at the liquid front bubbles are first compressed because of the increasing local liquid pressure gas bubble pressure is sufficiently high, gas dissolution induces the final bubble collapse Surprisingly, the bubbles' presence is found to have a very minor effect on nanoslits capillary filling kinetics bubbles are observed with all the liquids for $a=20$ nm. Bubbles created lastly have longer lifetime, the lifetime seems to depend on the initial bubble size (small bubbles disappear more rapidly) the increase in the liquid pressure as the distance between the front and the bubble location increases 	 <ul style="list-style-type: none"> the distance between liquid front and the nanoslit entrance is 750 micron Liquid appears as dark and gas (air) as white (flow from left to right)

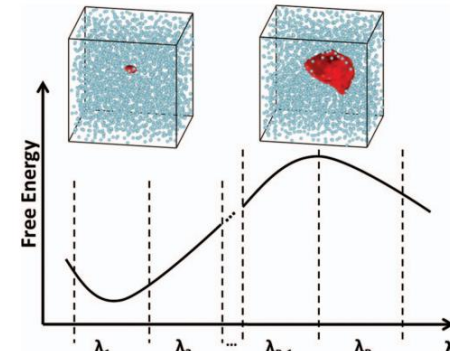

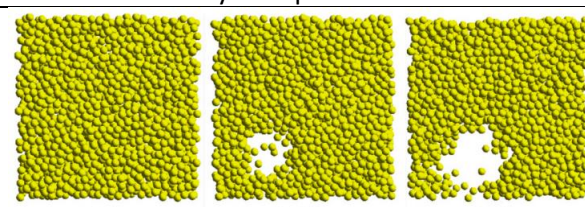
This document summarizes simulations/experimental setups in literature marking original targets and useful information.

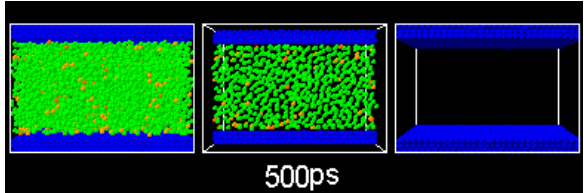
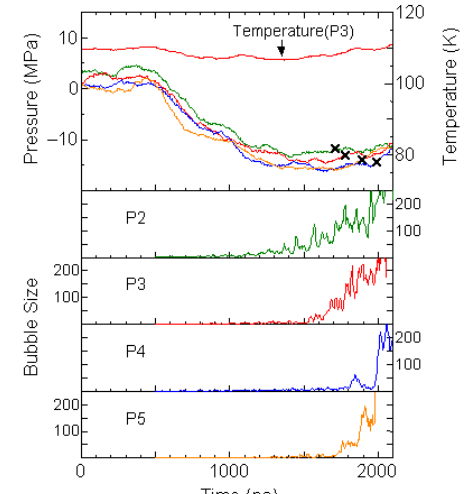
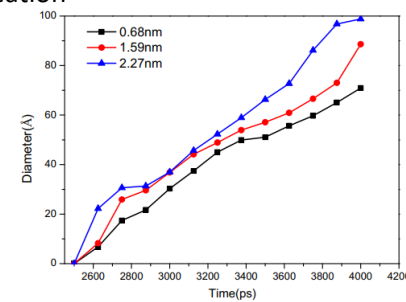
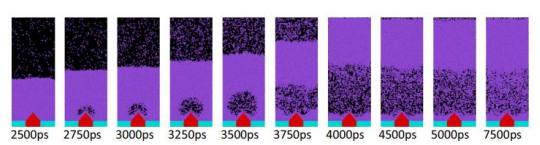
#	Short intro	Setup details	Outcomes	Related to us
7	<ul style="list-style-type: none"> how popular barostats behave when applied straightforwardly to heterogeneous systems homogeneous nucleation of a vapor bubble in a metastable liquid 	<ul style="list-style-type: none"> super-heated LJ liquid hybrid restrained Monte Carlo sharp-interface model M-method: Particles are labeled as liquid-like if they have more than five particles closer than 1.6σ, and vapor-like otherwise 		 <p>FIG. 3. Instantaneous bubble configurations corresponding to increasing bubble sizes (from left to right) at $T = 0.855$ and $P_L = 0.026$. The spheres represent the cells of the vapor cluster.</p>
8	<ul style="list-style-type: none"> two grid-based methods, the M-method and the V-method, to detect bubbles in metastable water 	<p>TIP4P/2005 model NPT, 2k particle, 2 fs, SHAKE T=NH@1ps, P=A@3ps=sound</p>	<ul style="list-style-type: none"> an order parameter to detect bubbles in water should meet the following criteria: <ul style="list-style-type: none"> should be local should not impose a specific shape should measure the “true” volume should be computationally inexpensive 	
9	<ul style="list-style-type: none"> bubble nucleation in metastable TIP4P/2005 water at negative pressure via MFPT 	<ul style="list-style-type: none"> TIP4P/2005 V-method bubbles by Voronoi SHAKE, NPT, 1fs, artificially empty spherical cavity by removing 30 water molecules $\sim 0.6 \text{ nm}$ cavity radius and a $0.90\text{--}0.95 \text{ nm}^3$ volume 	<ul style="list-style-type: none"> the mechanism of bubble formation above and below the spinodal <ul style="list-style-type: none"> above the spinodal line, one bubble grows larger than all others below the spinodal line, we detect the formation of few bubbles which, eventually, merge to form larger ones small bubbles are strongly fluctuating objects 	

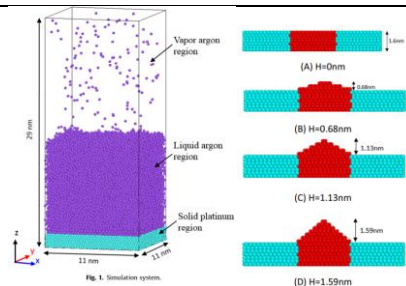
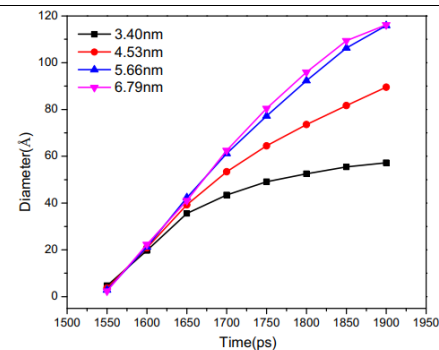
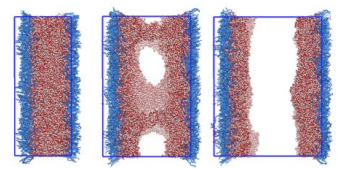
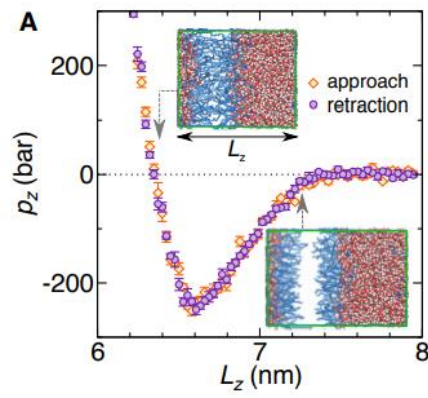
This document summarizes simulations/experimental setups in literature marking original targets and useful information.

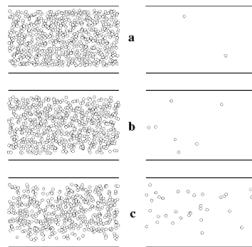
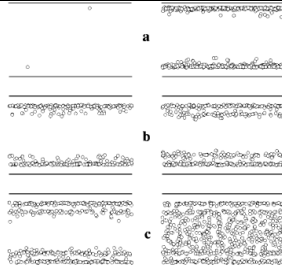
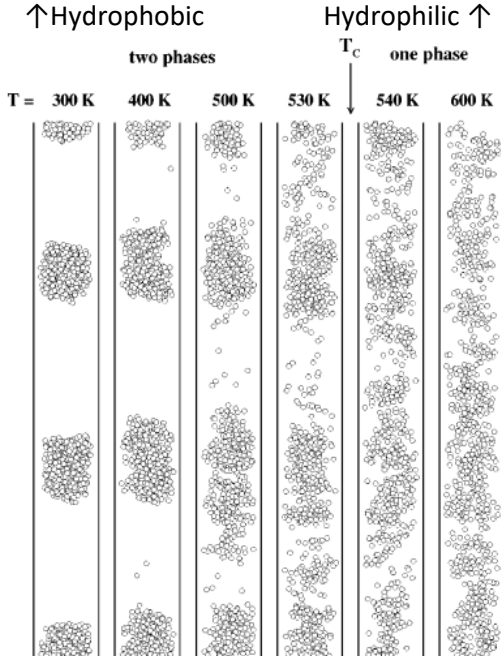
#	Short intro	Setup details	Outcomes	Related to us
10	<ul style="list-style-type: none"> the fluid-inclusion experiment large mechanical tension 	<ul style="list-style-type: none"> Heating vapor-liquid two phase system liquid is stretched 	<ul style="list-style-type: none"> cavitation statistics are characteristic of a thermally activated process both the free energy and the volume of the critical bubble are well described by classical nucleation theory when the surface tension is reduced by less than 10%, consistent with homogeneous cavitation 	 <ul style="list-style-type: none"> The LDM has been measured only down to -20.3 MPa at 280.84 K
11	<ul style="list-style-type: none"> homogeneous bubble nucleation in a Lennard-Jones fluid 	<ul style="list-style-type: none"> NPT cubic periodic boundary conditions MC assumes system is always locally in thermal equilibrium 	<ul style="list-style-type: none"> cavitation starts with compact bubbles rather than with ramified structures local temperature fluctuations correlate strongly with subsequent bubble formation CNT: the size of the critical bubble is inversely proportional to the degree of supersaturation 	 <p>Figure 4. Typical bubble-nucleation pathway in a superheated liquid</p> <ul style="list-style-type: none"> When a system undergoes a liquid-to-vapor transition during an NPT simulation, the simulation box tends to expand dramatically: in our simulation runs, we limit such “explosions” by interrupting the runs before the liquid phase has evaporated completely.
12	<ul style="list-style-type: none"> homogeneous liquid–vapor nucleation in the superheated LJ 	<ul style="list-style-type: none"> Monte Carlo simulations 	<ul style="list-style-type: none"> Small interstitial cavities present even in the equilibrium liquid. Much larger cavities that develop as the system climbs the nucleation free energy barrier average cavity size is a function of density but not of temperature weblike cavity is nonspherical at all superheating 	 <p>FIG. 5. Average cavity volume, $\langle V_{cav} \rangle$, as a function of the order parameter (reduced density) at three different superheatings, 8.2% (○), 9.1% (+), and 10.0% (▽). Note that all points fall on the solid line, an exponential fit of the data.</p> <p>FIG. 8. Cavity pockets in the equilibrium Lennard-Jones liquid at saturation ($P^* = 0.0463$, $T^* = 1.10$). Different cavities are denoted by different shading. Periodic boundary conditions are used. Full simulation box shown; actual atoms removed for clarity.</p>

This document summarizes simulations/experimental setups in literature marking original targets and useful information.

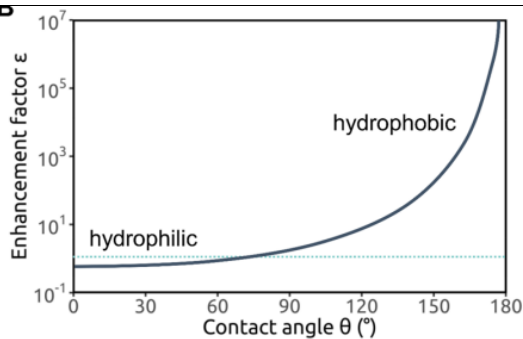
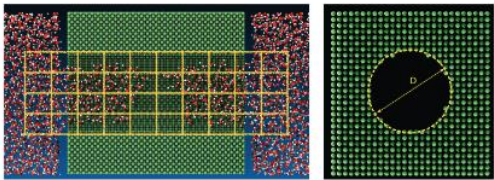
#	Short intro	Setup details	Outcomes	Related to us
13	<ul style="list-style-type: none"> homogeneous liquid to vapor nucleation 	<ul style="list-style-type: none"> LJ Periodic boundary conditions on a cubic simulation box 	<ul style="list-style-type: none"> bubble takes on cohesive non-spherical shapes with irregular and (sometimes highly) undulating surfaces 	 <p>FIG. 1. BXD divides the order parameter, λ, into B boxes to capture the metastable liquid basin at box 1 up to and past the transition state at box B. Bubbles shown in red, are small fluctuations that form and break up in the metastable liquid basin and grow to a critical size at the transition state.</p>  <p>FIG. 2. The evolution of a bubble in a stretched liquid ($W \approx 3$ to 125); from the initial formation at the top left to the critical bubble on the bottom right, the instantaneous shape that the bubble takes on during growth is irregular and non-spheroidal. These results are from a successful FFS trajectory and hence representative of a continuous dynamic process.</p> <ul style="list-style-type: none"> bubble volume is a more ideal reaction coordinate than global density to quantify the progression of the metastable liquid The timescale for the volume fluctuations is approximated as the length of the simulation box divided by the speed of sound in the fluid
14	<ul style="list-style-type: none"> homogeneous liquid–vapor nucleation for a LJ fluid 	<ul style="list-style-type: none"> uniformly and instantaneously expanded bulk NPT 	<ul style="list-style-type: none"> The first stage = nucleation: the pressure and temperature and potential energy are maintained nearly constant. The second stage = growth stage: the pressure and temperature increase rapidly and the potential energy decreases rapidly. 	 <p>t = 0 t = 100 t = 160</p>

#	Short intro	Setup details	Outcomes	Related to us
15		<ul style="list-style-type: none"> LJ liquid argon consisted of 5488 molecules solid surface = 3 layers of harmonic molecules (1020 molecules in each layer) in fcc (111) a quite wettable potential parameter ($\epsilon_{\text{INT}} = 0.894 \times 10^{-21}$ J) on the top surface tested different wettability on the bottom surface 	<ul style="list-style-type: none"> When the bottom surface is less wettable, the size of void seems to increase monotonically when the bottom surface is more wettable, no large void appeared until the sudden appearance of the void of about more that 100 expanded the system volume by moving the top surface at a constant speed 	<ul style="list-style-type: none"> applied three-dimensional grids of 2\AA intervals and visualized the grid as a 'void' when there were no molecules within $1.2\sigma_{\text{AR}}$  <p>↑The solid surface became more wettable from P2 to P5.</p>
16	<ul style="list-style-type: none"> bubble nucleation of ultra-thin liquid argon film on a platinum surface 	<ul style="list-style-type: none"> the liquid is heated by the middle part and cooled by the two sides of the platinum surface NVE the periodic boundary condition is applied in the x- and y-directions, and the upper boundary of z direction is the reflecting wall. surface wettability is strongly hydrophilic, and the contact angle is set to be 0 in all simulations 	<ul style="list-style-type: none"> nanostructure surface increases rate of nucleation  <p>Fig. 13. Growth trends of bubble nuclei above nanostructure surfaces with height of 0.68 nm, 1.59 nm and 2.27 nm.</p>	

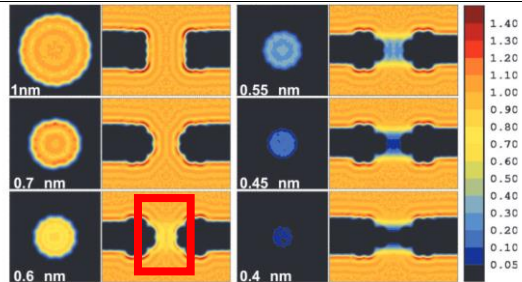
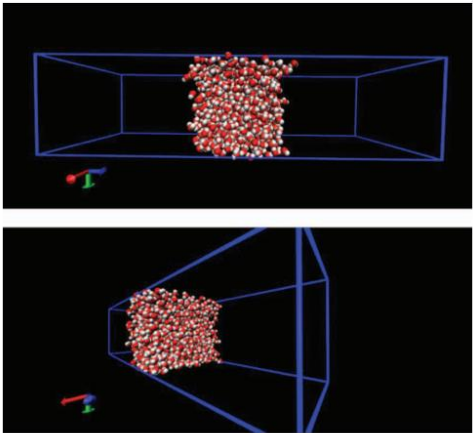
#	Short intro	Setup details	Outcomes	Related to us
		 <p>Fig. 1. Simulation system.</p>	 <p>Fig. 16. Growth trends of bubble nuclei above nanostructure surfaces with height of 3.40 nm, 4.53 nm, 5.66 nm, and 6.79 nm.</p>	
17		<ul style="list-style-type: none"> OPLS, cubic box 2ns simulation box size was increased by 1% and relax 1ns, to a total of 15% deformation 		an expansion rate of approximately 0.1 m/s
18	<ul style="list-style-type: none"> lipid bilayers and water, hydrophobic smooth surfaces 	 <p>Fig. S7. Stretching the water slab between two lipid monolayers by pulling them apart: the water slab cavitates in the middle.</p>		<ul style="list-style-type: none"> TIP4P/2005
19	<ul style="list-style-type: none"> Coexistence curves of water in cylindrical and slitlike nanopores of different size 	<ul style="list-style-type: none"> Monte Carlo simulations TIP4P cylindrical pores with radii r from 12 to 20 Å slitlike pores of width $H = 24$ Å 	<ul style="list-style-type: none"> A single liquid–vapor coexistence: hydrophobic and moderately hydrophilic pores the water–substrate interaction comparable or stronger than the water–water pair interaction: prewetting, one and two layering transitions 	

#	Short intro	Setup details	Outcomes	Related to us
			<div><div><p>FIG. 7. Arrangement of the water oxygens in the coexisting liquid and vapor phases in a hydrophobic slitlike pore with $H_p=24$ Å and $U_0=-0.39$ kcal/mol. (a) $T=200$ K; (b) $T=400$ K; (c) $T=530$ K.</p></div><div><p>FIG. 10. Arrangement of water oxygens in coexisting phases in the hydrophilic slitlike pore with $H_p=24$ Å and $U_0=-4.62$ kcal/mol. (a) First layering transition; (b) second layering transition; (c) liquid-vapor transition of the "inner" water.</p></div><div><p>↑Hydrophobic Hydrophilic ↑ two phases one phase T = 300 K 400 K 500 K 530 K 540 K 600 K T_c</p></div><div><p>FIG. 13. Arrangement of water oxygens in a hydrophobic cylindrical pore with radius $R_p=12$ Å, length $L=300$ Å, $U_0=-0.39$ kcal/mol and average density $\rho_C=0.218$ g cm⁻³ at various temperatures.</p></div></div>	

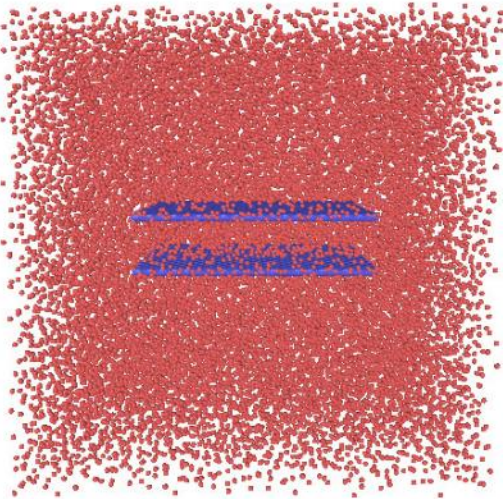
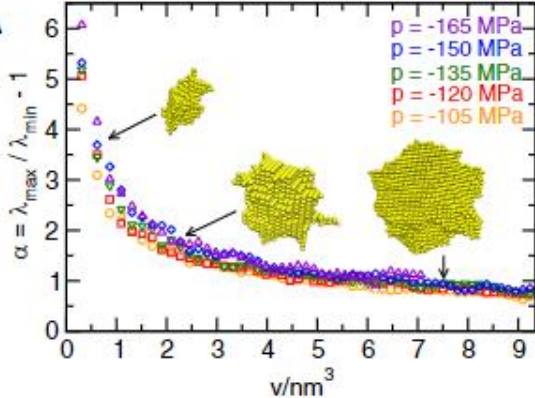
This document summarizes simulations/experimental setups in literature marking original targets and useful information.

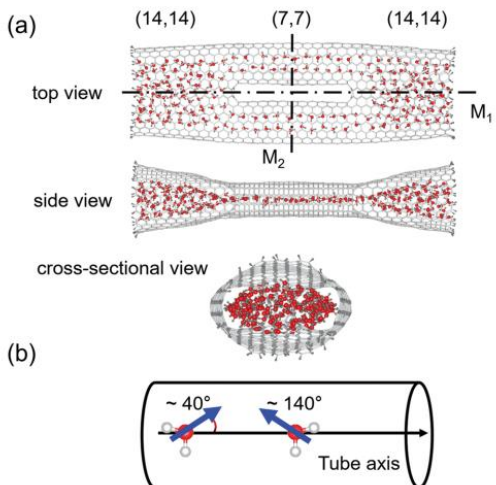
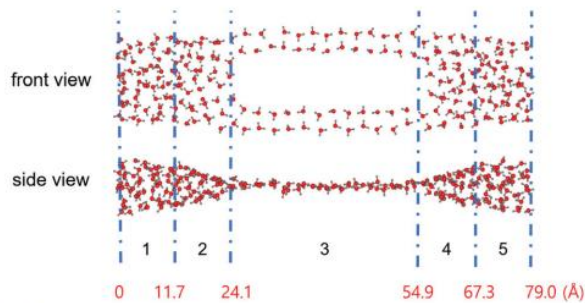
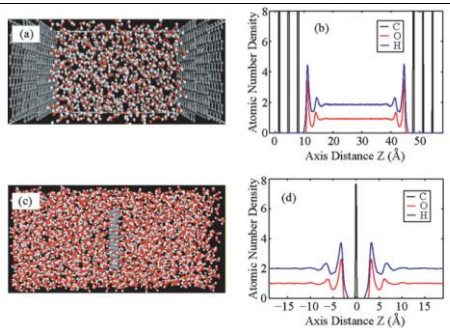
#	Short intro	Setup details	Outcomes	Related to us
20	<ul style="list-style-type: none"> Water in nanopores and biological channels 		 <ul style="list-style-type: none"> water flow enhancement factor (ϵ, defined as the ratio of the water flow to that predicted by the Hagen–Poiseuille equation for bulk water viscosity and no-slip boundary conditions) versus pore wall water contact angle for an $R = 4$ nm pore 	<ul style="list-style-type: none"> Water Models: TIP4P
21	<ul style="list-style-type: none"> Intrusion and extrusion of water in hydrophobic nanopores 	 <p>Fig. 1. System used in the atomistic string calculations; it comprises a nanopore excavated from a hydrophobic Lennard-Jones crystal and ca. 13,000 TIP4P/2005 molecules. (Left) The coarse-grained density field of water is computed on a grid of $4 \times 4 \times 10$ cubic cells with the sides measuring ca. 7 Å (yellow lines). Further details on the simulations and on the string method are found in Supporting Information. (Right) Definition of the pore diameter D adopted here, based on the center of the last wall atoms.</p> <ul style="list-style-type: none"> Single cylindrical nanopore, $D = 2.6$ nm Hydrophobic $\theta_v = 119$ TIP4P/2005, SHAKE, relax 3 ns pressure was kept constant by using two pistons Periodic boundary conditions were enforced in the y and z (orthogonal to the axis of the pore) pressure varied in steps by changing the force applied on the pistons 		<ul style="list-style-type: none"> Pressure was monitored by probing the stress tensor computed in two symmetrical boxes on the two sides of the nanoporous matrix, far enough from the solid walls to be considered a good estimator of the liquid pressure

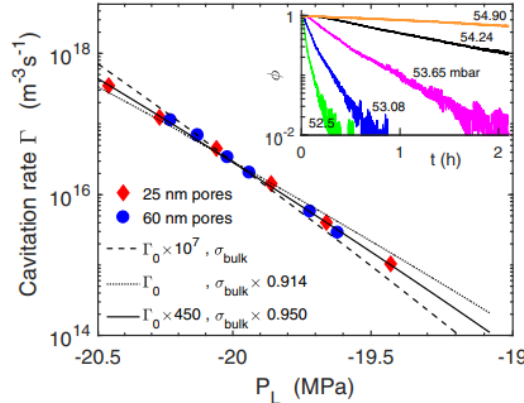
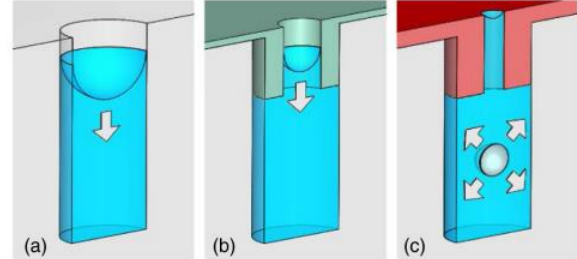
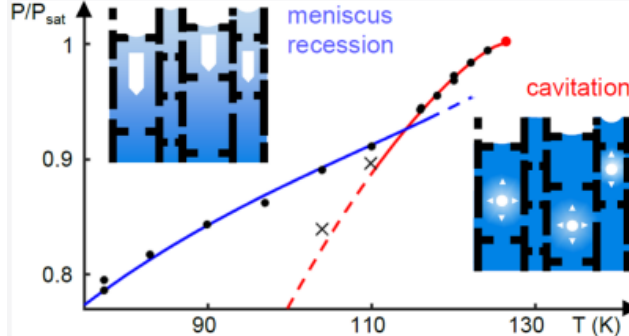
This document summarizes simulations/experimental setups in literature marking original targets and useful information.

#	Short intro	Setup details	Outcomes	Related to us
22	<ul style="list-style-type: none"> Liquid–vapor oscillations of water in hydrophobic nanopores 	<ul style="list-style-type: none"> Cylindrical pores with hydrophobic pseudo atoms Radius 1 - 0.4 nm, length 0.4 nm SPC water 	 <p>Fig. 2. Water density in hydrophobic pores with radii ranging from 1 to 0.4 nm. (Left) Density z-averaged over the length of the pore. (Right) Radially averaged density. The density is in units of SPC bulk water at 300 K and 1 bar [plots were prepared with <i>ovasp</i> v.1.0.2].</p>	
23	<ul style="list-style-type: none"> water's evaporation at its liquid/air interface 	<ul style="list-style-type: none"> SPC/E water  <p>FIG. 1. Rendering of 1025 water molecules in the $31 \times 31 \times (4 \times 31 \text{ Å})$ unit cell. The z-axis is in the horizontal direction.</p>	<ul style="list-style-type: none"> tends to rotate so that its dipole and one O–H bond are oriented outward as it crosses the Gibbs dividing surface 	
24	<ul style="list-style-type: none"> liquids in a graphene (hydrophobic) slit pore 	<ul style="list-style-type: none"> TIP4P/2005 water, NVT 	<ul style="list-style-type: none"> water has a large increase in diffusion for subnm slit pores, becoming faster than bulk 	

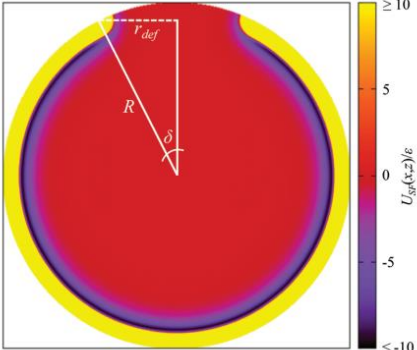
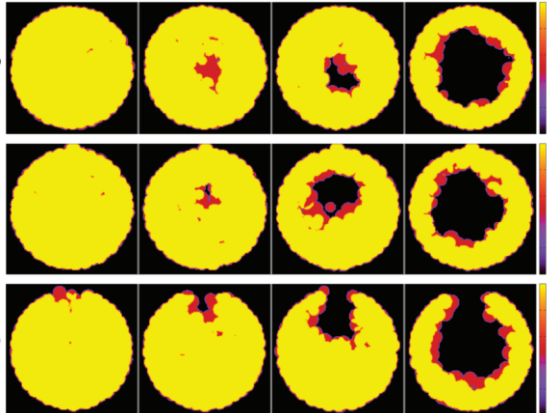
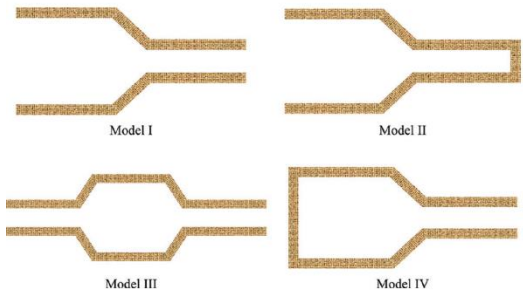
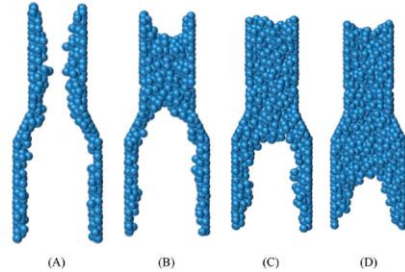
This document summarizes simulations/experimental setups in literature marking original targets and useful information.

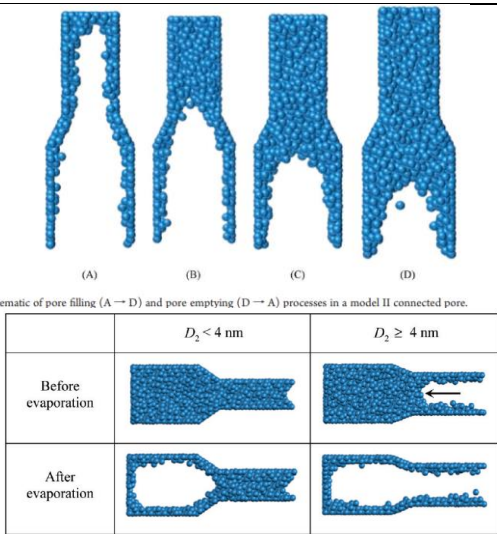
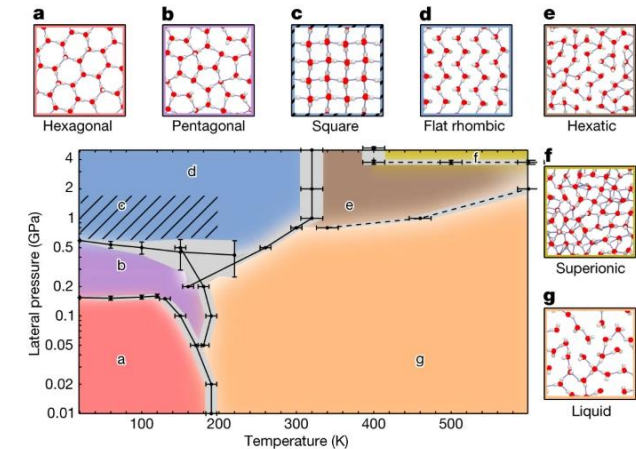
#	Short intro	Setup details	Outcomes	Related to us
				
25	<ul style="list-style-type: none">cavitation in water under tension	<ul style="list-style-type: none">hMC, TIP4P	<ul style="list-style-type: none">in the early stages of cavitation, bubbles are irregularly shaped and become more spherical as they grow  <p>↑asphericity α as a function of bubble volume</p>	

#	Short intro	Setup details	Outcomes	Related to us
26	<ul style="list-style-type: none"> Equilibrium structures of water molecules confined 	<p>(a)</p>  <p>Fig. 1 (a) A model structure of the MCCNT that contains the water molecules for the TIP3P model (a snapshot at 20 ns). (b) Schematic illustration of the orientation of the dipole moment of an H₂O molecule.</p>	 <p>Fig. 3 Snapshot of the result of simulating the behaviour of water molecules in the MCCNT at 280 K for 20 ns with TIP3P water. The MCCNT structure is omitted for clarity. The blue dashed line separates the regions, as indicated in Table 1. Numbers in red indicate the distance from the left end of the MCCNT.</p>	
27	<ul style="list-style-type: none"> interaction of interfacial water vs hydrophobicity of epitaxial graphene 	<ul style="list-style-type: none"> graphene sheets as mesoscopic slit pores periodic in all three dimensions slit size of 4 nm SPC water / TIP3P 	 <p>FIG. 4. (Color online) Classical MD simulations of graphene in contact with water. (a) Classic MD simulation of water under confinement between graphene sheets (finite-size slit-pore). The water structure resembles the case of bulk water for the slit size of 4 nm in this study. (b) The resultant number density profiles of respective atoms as a function of axis distance. (c) Isobaric-isothermal MD simulation of water at the fluid-graphene interfaces (a free-standing sheet). (d) The number density profiles of respective atoms as a function of axis distance.</p>	

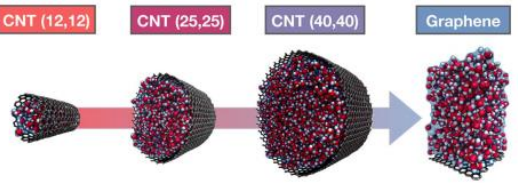
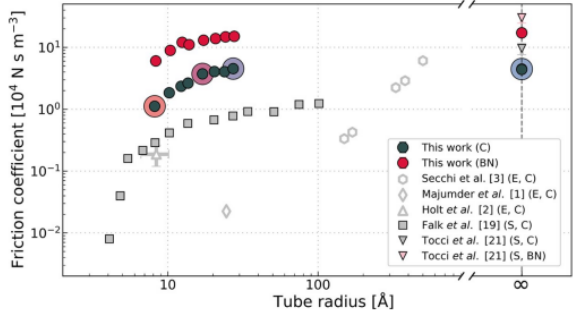
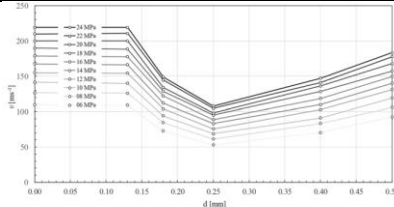
#	Short intro	Setup details	Outcomes	Related to us
28	<ul style="list-style-type: none"> Direct observation of homogeneous cavitation 	<ul style="list-style-type: none"> Hexane from porous alumina and silicon membranes 	 <p>FIG. 4. Cavitation rate Γ at 19°C as a function of liquid pressure P_L for poAl membranes with average pore diameters $d = 60$ nm and $d = 25$ nm. Here, Γ is measured from the exponential decay of the number of filled pores following a quench of the pressure reservoir from 60 mb down to a lower pressure ranging between 52 and 55 mbar, as illustrated in the inset for the 60-nm membrane. The fraction of filled pores ϕ is measured through the logarithm of the optical transmission and normalized to its value at time $t = 0$, corresponding to a 10% transmission [20]. The cavitation rate per unit volume Γ is deduced by dividing the decay rate by the pore volume, which is computed using $d = 56$ nm and $d = 27$ nm. These values lie within the error bars of the measured values above and are such that $\Gamma(P_L)$ is identical for the two membranes. Lines correspond to the CNT predictions for different values of the attempt rate or the surface tension (see text).</p>	 <p>FIG. 1. Cavitation in an ink-bottle geometry. (a) Straight cylindrical pore opened to a vapor reservoir, which empties through recession of the liquid-vapor meniscus. The smaller the pore diameter, the smaller the evaporation pressure. (b,c) Two possible evaporation mechanisms for a cavity ended by a cylindrical constriction. In panel (b), the constriction empties at its equilibrium pressure, triggering further evaporation in the wider cavity through meniscus recession; in panel (c), if the constriction is narrow enough for its evaporation pressure to lie below the cavitation threshold, the cavity empties by cavitation, while the constriction remains filled with liquid.</p>
29	<ul style="list-style-type: none"> Sorption isotherms for helium and nitrogen for a series of porous silicon 			

#	Short intro	Setup details	Outcomes	Related to us																				
30	<ul style="list-style-type: none">drying dynamics of porous media with two pore diameters separated by several orders of magnitude	<ul style="list-style-type: none">extreme ink-bottle structure—large pore bodies connected via narrow throat	<div><div>(a) </div><div>(b) </div><div>(c) </div><div>(d) </div></div>																					
31	<ul style="list-style-type: none">GCMC simulations of argon adsorption in slit pores of different channel geometry	<div><div></div><div></div><div></div><div></div></div> <p>Figure 1. Configurations of the four solid models: (a) finite slit pore, (b) finite slit pore with one close end, (c) two connected pores exposed to bulk, and (d) cavity connected to smaller necks.</p>	<div><div></div><div></div></div> <p>Figure 5. Schematic diagram showing the advance of different interfaces in (a) a slit pore with two ends open to the bulk phase and (b) a slit pore with one end closed. Pressure increases from left to right.</p> <div><div></div><div></div></div> <p>Figure 7. Schematic diagram of the advancing of interfaces in short and longer pores: (a) dominated by a semicylindrical interface in the short large pore and (b) dominated by a flat interface in the long large pore.</p>	<table><tr><th>Hysteresis type</th><th>Isotherm</th><th>Configuration of the pore</th></tr><tr><td rowspan="5">H1</td><td></td><td></td></tr><tr><td></td><td></td></tr><tr><td></td><td></td></tr><tr><td></td><td></td></tr><tr><td></td><td></td></tr><tr><td>H5</td><td></td><td></td></tr><tr><td>H6</td><td></td><td></td></tr></table>	Hysteresis type	Isotherm	Configuration of the pore	H1											H5			H6		
Hysteresis type	Isotherm	Configuration of the pore																						
H1																								
H5																								
H6																								

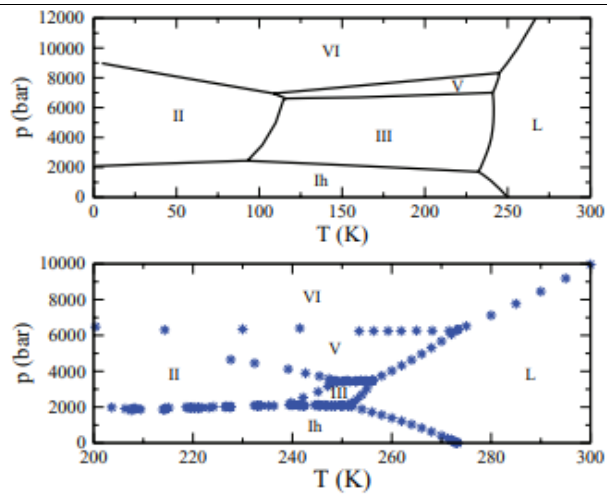
#	Short intro	Setup details	Outcomes	Related to us
32	<ul style="list-style-type: none">onset of cavitation in a metastable fluid confined to nanoscale pores with nonwetting defects	<ul style="list-style-type: none">Monte Carlo simulations LJ fluid in a spherical poresite-averaged LJ potentialA nonwetting defect of variable size was introduced as a round spot on the pore wall which does not exert the attractive potential  <p>Figure 3. The solid–fluid potential energy map on the xz-plane of a 5.54 nm pore with a 2.21 nm nonwetting defect introduced. Overlay: geometry of eqs 8 and 10.</p>	 <p>Figure 7. Snapshots of growing bubbles quantified by the particle probabilities on the xz-plane during desorption; yellow indicates the probability of unity and black the probability of zero. (a) Pore without defect shows the nucleation of the critical cavity at the center of the pore. (b) Pore with a small defect (0.40 nm) still exhibits homogeneous nucleation. (c) Pore with 1.85 nm defect exhibits a flat interface at complete pore filling, followed by the growth the bubble pinned to the defect; this bubble grows until the vapor-like state is reached.</p>	
33	<ul style="list-style-type: none">GCMC simulation of argon adsorption in connected cylindrical pores	 <p>Model I Model II</p> <p>Model III Model IV</p>	 <p>(A) (B) (C) (D)</p> <p>Figure 5. Schematic illustration of the pore filling process ($A \rightarrow D$) and pore emptying process ($D \rightarrow A$) in a model I connected pore.</p>	

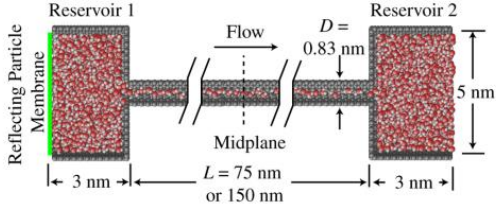











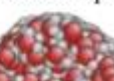
#	Short intro	Setup details	Outcomes	Related to us									
			<div><table data-bbox="1079 497 1574 721"><tr><th></th><th>$D_2 < 4 \text{ nm}$</th><th>$D_2 \geq 4 \text{ nm}$</th></tr><tr><td>Before evaporation</td><td></td><td></td></tr><tr><td>After evaporation</td><td></td><td></td></tr></table></div>		$D_2 < 4 \text{ nm}$	$D_2 \geq 4 \text{ nm}$	Before evaporation			After evaporation			
	$D_2 < 4 \text{ nm}$	$D_2 \geq 4 \text{ nm}$											
Before evaporation													
After evaporation													
	<ul style="list-style-type: none">a single layer of water within a graphene-like channel	<ul style="list-style-type: none">machine learning potential	<div><p>Fig. 1: Phase diagram of monolayer nanoconfined water.</p><p>a–g. The pressure–temperature phase diagram of monolayer water was calculated using an MLP that delivers first-principles accuracy. The solid and dashed lines indicate first-order and continuous phase transitions, respectively. The grey regions indicate the statistical uncertainty for solid–solid phase transitions and, for the other transitions, the uncertainties arising from studying a finite number of thermodynamic states. The diagonally hatched area indicates the region in which square and flat-rhombic phases are near degenerate. Diagrams of the hexagonal (a), pentagonal (b), square (c), flat-rhombic (d), hexatic (e), superionic (f) and liquid (g) phases are shown with oxygen atoms in red, hydrogen atoms in grey and hydrogen bonds shown by blue lines.</p></div>										

This document summarizes simulations/experimental setups in literature marking original targets and useful information.

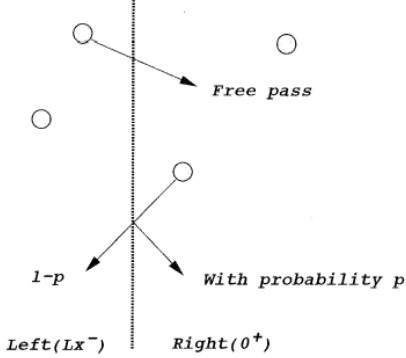
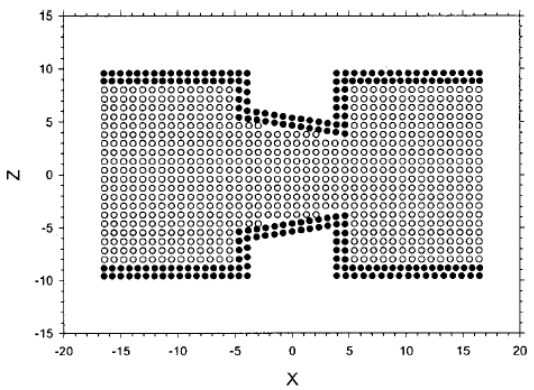
#	Short intro	Setup details	Outcomes	Related to us
35	<ul style="list-style-type: none"> machine learning-based molecular dynamics simulations water transport in single-wall carbon and boron nitride nanotubes 			
36	<ul style="list-style-type: none"> Evaporation driven pumping 	<ul style="list-style-type: none"> micro-channels were 110 mm wide, 28 mm deep and 4 or 10 cm long 	<ul style="list-style-type: none"> continuous liquid transport velocity of up to 2.25 mm/s 	<ul style="list-style-type: none"> The pump demonstrated in this paper operates only in the positive pressure domain.
37	<ul style="list-style-type: none"> cross-sectional speed of water flow in narrow cylindrical metal tubes at high pressure 		 <p>Figure 2. Dependence of the mean cross-sectional flow speed v in metal tubes of length 20 mm with internal diameter d for input pressure $p = (6, 8, 10, 12, 14, 16, 18, 20, 22, 24)$ MPa from values in Table 1.</p>	
38	<ul style="list-style-type: none"> homogeneous bubble nucleation in a LJ liquid under a negative pressure 	<ul style="list-style-type: none"> cubic cell with periodic boundary conditions NVE method of mean lifetime stretching (scaling of all the particle coordinates in the cell) 		
39	<ul style="list-style-type: none"> bubble nucleation in LJ liquid 	<ul style="list-style-type: none"> cubic cell with periodic boundary conditions NVE 		
40	<ul style="list-style-type: none"> phase diagram of water at negative pressures 	<ul style="list-style-type: none"> two models of water, TIP4P/2005 and TIP5P 	<ul style="list-style-type: none"> care that must be taken with nucleation studies carried out with TIP5P 	<ul style="list-style-type: none"> TIP4P/2005

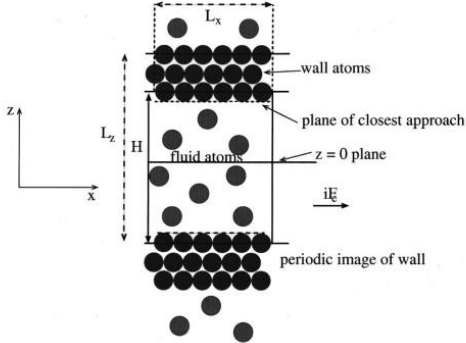
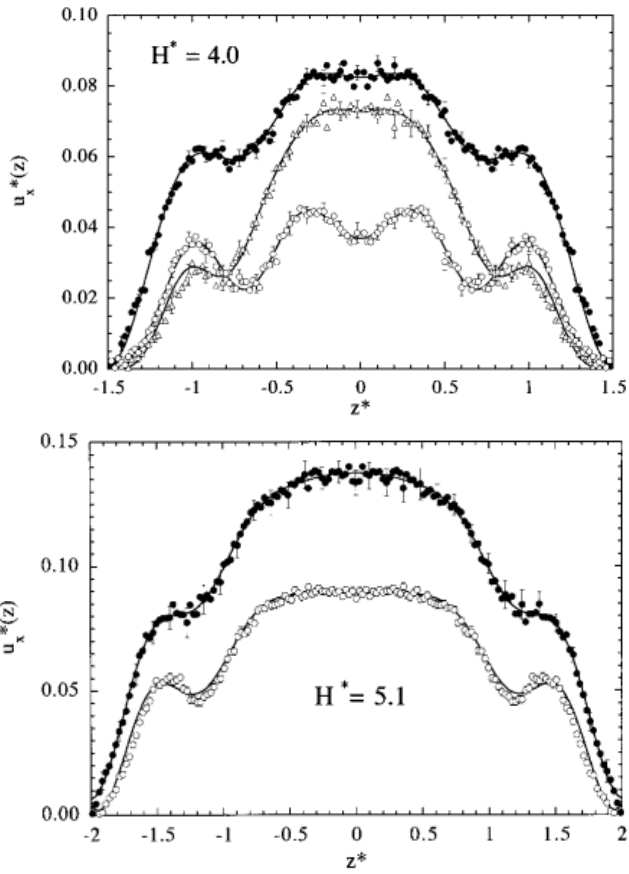
This document summarizes simulations/experimental setups in literature marking original targets and useful information.

#	Short intro	Setup details	Outcomes	Related to us																																								
41	<ul style="list-style-type: none"> simulated values of the surface tension 		<ul style="list-style-type: none"> The SPC/E and TIP6P models provide the best agreement with experiment <p>TABLE I. Simulated surface tensions (γ in mN/m) of various water models as a function of temperature. Experimental data were taken from Ref. 10 and can be represented by the equation $\gamma(T)=94.74+1.87\times 10^{-3}T-2.63\times 10^{-4}T^2$ between 273 and 373 K. Typical estimated errors in the simulated values were 1–2 mN/m.</p> <table border="1"> <thead> <tr> <th>Model</th><th>275 K</th><th>300 K</th><th>325 K</th><th>350 K</th></tr> </thead> <tbody> <tr> <td>TIP3P</td><td>54.0</td><td>49.5</td><td>44.5</td><td>41.7</td></tr> <tr> <td>SPC</td><td>59.7</td><td>53.4</td><td>49.0</td><td>45.5</td></tr> <tr> <td>SPC/E</td><td>64.5</td><td>61.3</td><td>58.0</td><td>52.7</td></tr> <tr> <td>TIP4P</td><td>61.0</td><td>54.7</td><td>50.8</td><td>46.7</td></tr> <tr> <td>TIP5P</td><td>57.1</td><td>52.3</td><td>46.1</td><td>42.4</td></tr> <tr> <td>TIP6P</td><td>64.8</td><td>61.8</td><td>55.4</td><td>52.8</td></tr> <tr> <td>Expt.</td><td>75.4</td><td>71.6</td><td>67.6</td><td>63.2</td></tr> </tbody> </table>	Model	275 K	300 K	325 K	350 K	TIP3P	54.0	49.5	44.5	41.7	SPC	59.7	53.4	49.0	45.5	SPC/E	64.5	61.3	58.0	52.7	TIP4P	61.0	54.7	50.8	46.7	TIP5P	57.1	52.3	46.1	42.4	TIP6P	64.8	61.8	55.4	52.8	Expt.	75.4	71.6	67.6	63.2	<ul style="list-style-type: none"> TIP4P/2005
Model	275 K	300 K	325 K	350 K																																								
TIP3P	54.0	49.5	44.5	41.7																																								
SPC	59.7	53.4	49.0	45.5																																								
SPC/E	64.5	61.3	58.0	52.7																																								
TIP4P	61.0	54.7	50.8	46.7																																								
TIP5P	57.1	52.3	46.1	42.4																																								
TIP6P	64.8	61.8	55.4	52.8																																								
Expt.	75.4	71.6	67.6	63.2																																								
42	<ul style="list-style-type: none"> MC for liquid water using simple intermolecular potentials 		<ul style="list-style-type: none"> Overall, the SPC, ST2, TIPS2, and TIP4P models give reasonable structural and thermodynamic descriptions of liquid water 	<ul style="list-style-type: none"> TIP4P/2005 																																								
43	<ul style="list-style-type: none"> coexistence simulations between the fluid and solid phases 		 <p>FIG. 6. Phase diagram for the TIP4P/2005 water model (top) compared with the experimental phase diagram (bottom).</p>	<ul style="list-style-type: none"> TIP4P/2005 																																								
44	<ul style="list-style-type: none"> x-ray scattering 		<ul style="list-style-type: none"> SPC/E and TIP4P give good agreement with our ALS experiment 	<ul style="list-style-type: none"> TIP4P/2005 																																								

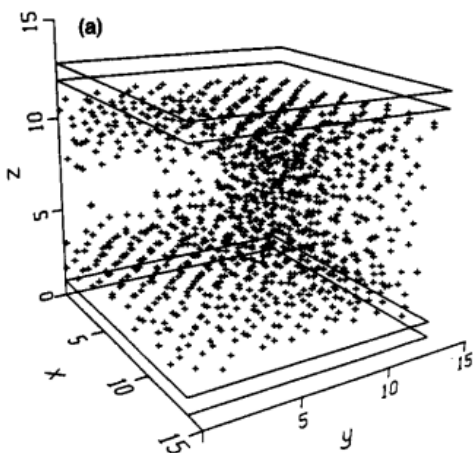
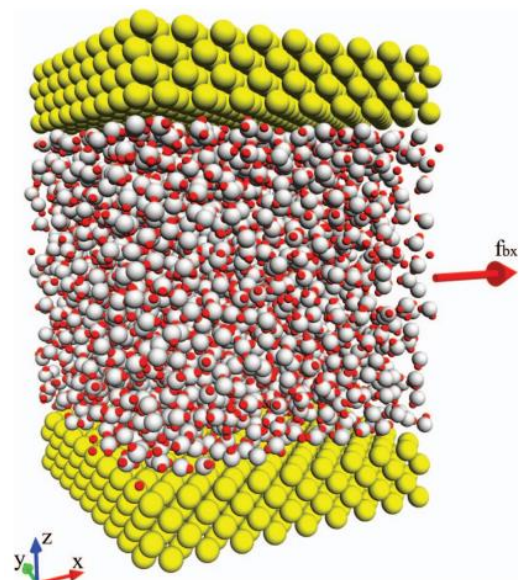
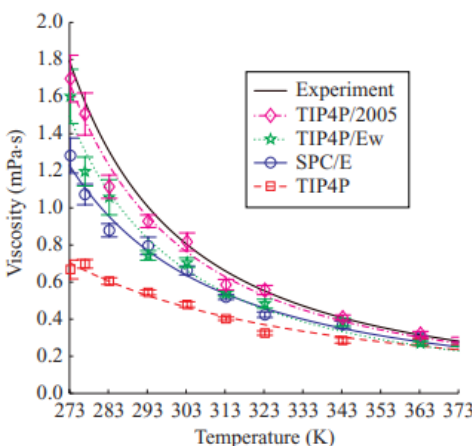
#	Short intro	Setup details	Outcomes	Related to us
45	<ul style="list-style-type: none"> pressure-driven water flow 	<ul style="list-style-type: none"> 75 and 150 nm-long carbon nanotubes with diameters ranging from 0.83 to 1.66 nm flow is driven by a reflecting particle membrane placed between the reservoirs  <p>FIG. 1 (color online). Snapshot from a typical flow simulation for the 0.83 nm-diameter CNT. A constant pressure difference is established between the reservoirs using a reflecting particle membrane. After a 0.25 ns initialization period, the mean pressure in each reservoir remains constant over the duration of the ensuing data collection period and flow through the tube is steady. Periodic boundary conditions are imposed in the flow direction. The number of molecules inside the CNT ranges from 310 ± 5 for the 75 nm-long, 0.83 nm-diameter CNT to 3676 ± 20 for the 150 nm-long, 1.66 nm-diameter CNT.</p>	<p>(a) Simulation Snapshot</p> <p>0.83 nm (6,6): single-file chain</p>   <p>0.96 nm (7,7): tilted pentagons</p>   <p>1.10 nm (8,8): stacked pentagons</p>   <p>1.25 nm (9,9): stacked hexagons</p>   <p>1.39 nm (10,10): bulklike liquid</p>   <p>1.66 nm (12,12): bulklike liquid</p>  	<ul style="list-style-type: none"> $\Delta P = P_1 - P_2$, where both are positive in the paper., and Δ can be negative but not P themselves as in the paper. Negative P can be induced in the reservoir if it is expanded as in bulk in the other two directions, or particles being removed.
46	<ul style="list-style-type: none"> ↑ Reflecting particle method 	<ul style="list-style-type: none"> perturbations to particle dynamics will decay over a distance of a few mean free 	<ul style="list-style-type: none"> old: 	<ul style="list-style-type: none"> a fictitious membrane to act as a filter to allow atoms crossing from one direction to

This document summarizes simulations/experimental setups in literature marking original targets and useful information.

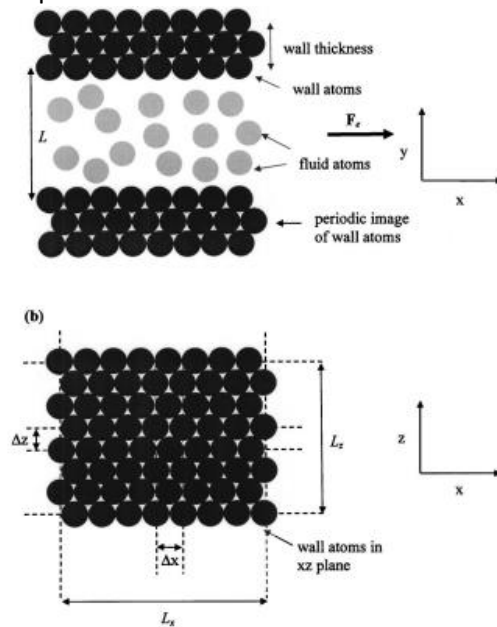
#	Short intro	Setup details	Outcomes	Related to us
		<p>paths, thus setting a lower limit for the C-A separation</p>  <p>FIG. 1. The reflecting particle method. If a fluid atom crosses $x=0$ from left ($x=L_x^-$) to right ($x=0^+$), it passes through 100%; but if it crosses $x=0$ from right to left, then it could be elastically reflected with probability p. The membrane is otherwise transparent in the sense that particles on two sides can interact.</p>	<ul style="list-style-type: none"> ○ 1: a constant artificial acceleration field is imposed on all the atoms of the fluid ○ 2: source and sink, at the two ends of the simulation cell, are maintained at different pressures 	<p>pass through without hindrance, while atoms crossing from the other direction are elastically reflected with a certain probability p</p>
47	<ul style="list-style-type: none"> • complex nano channel flow 	<ul style="list-style-type: none"> • At the beginning without applying the external force • external force field as gravity field on a molecule to produce a flow in the x-direction, • Periodic boundary conditions are applied  <p>FIG. 1. Initial configuration of wall and fluid molecules.</p>	<ul style="list-style-type: none"> • Nano-sized vortex flow can be developed at low Reynolds numbers due to near-wall molecules having large enough momenta, resulting in qualitatively different flow field from that predicted by the Navier–Stokes equations 	<ul style="list-style-type: none"> • Applying a force to all particles

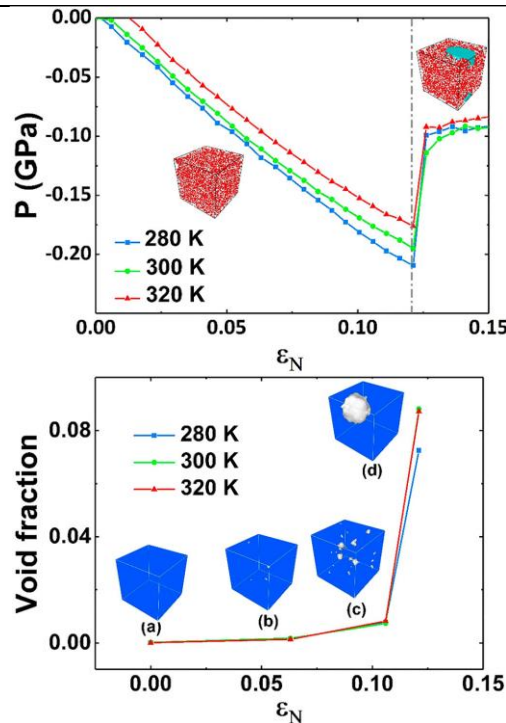
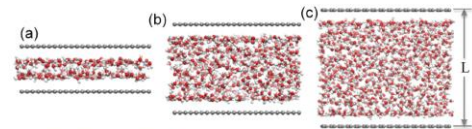
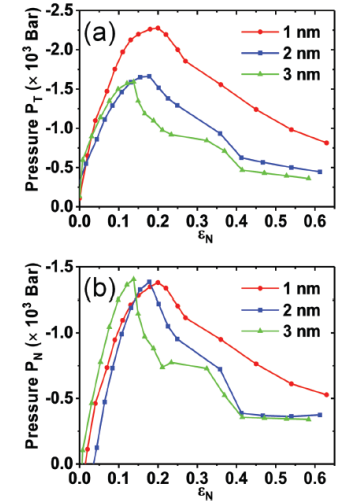
#	Short intro	Setup details	Outcomes	Related to us
48	<ul style="list-style-type: none"> LJ fluids in narrow slit pores 	<ul style="list-style-type: none"> we apply a constant force in the x direction to each particle  <p>FIG. 1. Simulation geometry for planar Poiseuille flow. The y-axis is normal to the page.</p>		
49	<ul style="list-style-type: none"> fluid flow at solid surfaces 	<ul style="list-style-type: none"> wall heavy mass, $m = 10^{10}m$, but allow these to move applying a uniform acceleration parallel to the walls 	<ul style="list-style-type: none"> How define walls: <ul style="list-style-type: none"> Fixed/frozen Solid molecules Site average 10-4 Lennard-Jones wall Boltzmann weighted wall, deeper, broader, and softer than 10-4 Inifnit wall potential for liquid molecule strays into the wall and zero otherwise 	

This document summarizes simulations/experimental setups in literature marking original targets and useful information.

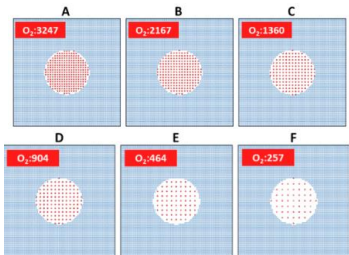
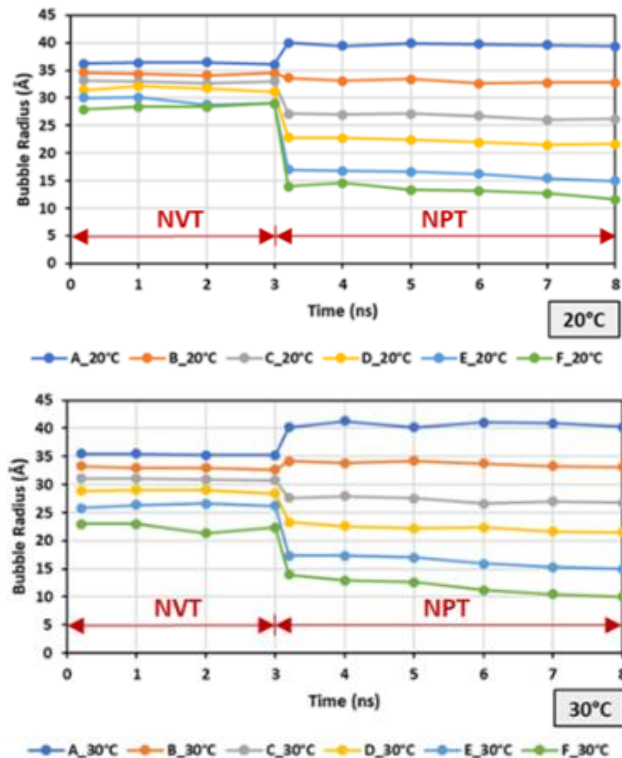
#	Short intro	Setup details	Outcomes	Related to us
				
50	<ul style="list-style-type: none">viscosity for several water models	<ul style="list-style-type: none">flow is generated by a constant body force f_{bx} in the x-direction on each molecule 	<ul style="list-style-type: none">The results show that the TIP4P/2005 model gives the best prediction 	<ul style="list-style-type: none">TIP4P

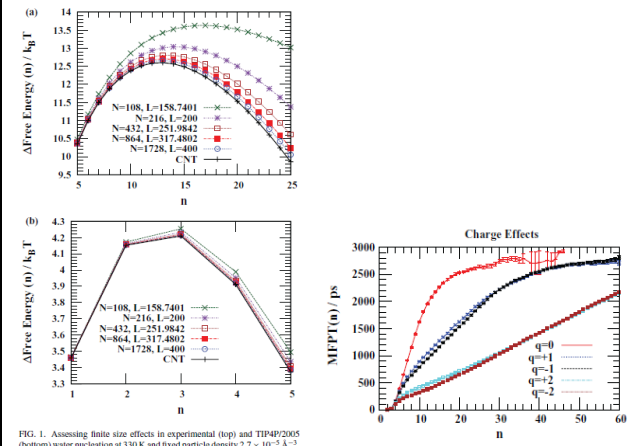
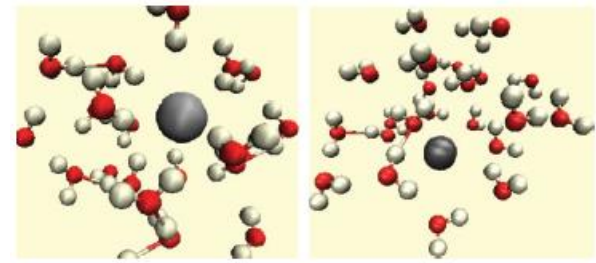
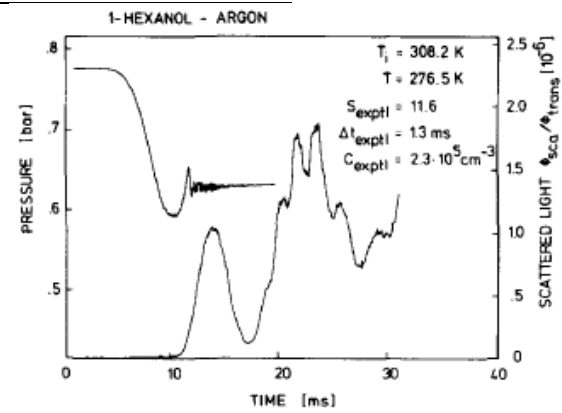
This document summarizes simulations/experimental setups in literature marking original targets and useful information.

#	Short intro	Setup details	Outcomes	Related to us												
51	<ul style="list-style-type: none">viscosity of confined inhomogeneous nonequilibrium fluids	<ul style="list-style-type: none">To generate Poiseuille flow, we apply a constant force (pressure head) in the positive x direction to all fluid atoms  <p>FIG. 1. Geometry of the simulation environment. (a) Overall system including fluid and wall atoms (z-direction normal to page); (b) wall atoms in the xz plane, defining separation of layers (y-direction normal to page).</p>		<ul style="list-style-type: none">The magnitude of the pressure head used in this work was $F_e=0.02$ for all systems studied.												
52	<ul style="list-style-type: none">shear viscosity of rigid water models		<ul style="list-style-type: none">In accordance with experimental data, TIP4P/2005 <p>TABLE I. Shear viscosities (in mPa s) of several rigid water models at 298 K and 1 bar.</p> <table><tr><th>TIP3P</th><th>TIP4P</th><th>TIP5P</th><th>SPC/E</th><th>TIP4P/2005</th><th>Expt.^a</th></tr><tr><td>0.321</td><td>0.494</td><td>0.699</td><td>0.729</td><td>0.855</td><td>0.896</td></tr></table> <p>^aReference 26.</p>	TIP3P	TIP4P	TIP5P	SPC/E	TIP4P/2005	Expt. ^a	0.321	0.494	0.699	0.729	0.855	0.896	
TIP3P	TIP4P	TIP5P	SPC/E	TIP4P/2005	Expt. ^a											
0.321	0.494	0.699	0.729	0.855	0.896											

#	Short intro	Setup details	Outcomes	Related to us
53	<ul style="list-style-type: none"> stretched water – bulk 	<ul style="list-style-type: none"> To simulate the stretched water, like the experimental process of metastable vapour-liquid equilibration, we removed a few water molecules gradually from the initial water box to generate different stretched extents 		
54	<ul style="list-style-type: none"> ↑stretched water – slit pore 	<ul style="list-style-type: none"> To generate different stretching extents of water in nanochannels, a few water molecules were removed randomly from the channels  <p>Fig. 1 A schematic diagram of water molecules confined within two parallel graphene sheets with a distance of (a) $L = 1$ nm, (b) $L = 2$ nm and (c) $L = 3$ nm. Carbon, oxygen and hydrogen atoms are represented by spheres in grey, red and white, respectively.</p>	 <p>Fig. 2 (a) Tangential pressure (P_T) and (b) the pressure normal to the wall (P_N) of confined water inside various graphene channels of $L = 1, 2$ and 3 nm as a function of stretching coefficient.</p>	

This document summarizes simulations/experimental setups in literature marking original targets and useful information.

#	Short intro	Setup details	Outcomes	Related to us
55	<ul style="list-style-type: none"> system size beyond which finite-size effects are expected to be negligible 	<p>For a given system, we can simply look at the error as a function of N at the density or supersaturation of interest</p>	<ul style="list-style-type: none"> If NVT → significant errors in the simulation and even to the impossibility of observing nucleation in a small finite system 	<ul style="list-style-type: none"> Optimization of the system size
56	<ul style="list-style-type: none"> bulk nanobubbles 	 <p>Snapshots A-F show nanobubbles with O₂ concentrations: A (3247), B (2167), C (1360), D (904), E (464), and F (257).</p>	 <p>The graphs show Bubble Radius (Å) vs Time (ns) for 20°C and 30°C. The NVT region is marked from 0 to 3 ns, and the NPT region is marked from 3 to 8 ns. The legend indicates data for A_20°C, B_20°C, C_20°C, D_20°C, E_20°C, and F_20°C.</p>	
57	<ul style="list-style-type: none"> nucleation rates from MD 	<ul style="list-style-type: none"> LJ argon as example 	<ul style="list-style-type: none"> Overall, the Mean first-passage time method (MFPT) and the Yasuoka–Matsumoto method (YM) seem to be the better choices. 	

#	Short intro	Setup details	Outcomes	Related to us
58	<ul style="list-style-type: none"> finite size effects, thermostats, and charged species 	<ul style="list-style-type: none"> TIP4P/2005 water in cubic box and periodic boundary conditions SETTLE for water, NVT, NVE, for condensation: NVT 	 <p>FIG. 1. Assessing finite size effects in experimental (top) and TIP4P/2005 (bottom) water nucleation at 330 K and fixed particle density $2.7 \times 10^{-3} \text{ Å}^{-3}$. Free energy profiles as a function of the cluster size n according to classical nucleation theory [Eq. (19)] (CST in legend) and the modified liquid drop model [Eq. (20)] (σ and L values, in legend). At this particle density, the experimental water has a supersaturation of $S = 7.146$ (top) while the TIP4P/2005 water model exhibits a supersaturation of $S = 25.735$ (bottom).</p> <p>FIG. 4. MFPTs as a function of cluster size n for 216 TIP4P/2005 water molecules at 330 K in a cubic box of side length 200 Å in presence of a single ion of varying charge. Each curve is an average over 600 independent trajectories.</p>	 <p>FIG. 5. Snapshots (created with the visualization program VMD⁷⁵) of the embryo after 2 ns of MD simulation at 330 K. Nucleation centers: monovalent anion (left), monovalent cation (right). The “M” sites and other TIP4P/2005 water molecules have been removed for clarity. The ion is depicted as a big gray sphere.</p>
59	<ul style="list-style-type: none"> Measurement of homogeneous nucleation rates via expansion chamber 	<ul style="list-style-type: none"> 1984 n-nonane nucleated on and droplet growth spring-operated pistons moving 	 <p>FIG. 4. Typical result of a single measuring run. Total gas pressure p (upper curve) and normalized scattered light flux $\Phi_{\text{sca}}/\Phi_{\text{trans}}$ for forward scattering angle 15° (lower curve) as functions of time.</p>	

[illegible]